

# Laue gamma-ray lenses: status and prospects

Filippo Frontera<sup>1</sup> and Peter von Ballmoos<sup>2</sup>,

<sup>1</sup>University of Ferrara, Physics Department, Via Saragat 1, 44100 Ferrara, Italy;

<sup>2</sup>Centre d'Etude Spatiale des Rayonnements, 9, Avenue du Colonel Roche, 31028 Toulouse, France

## ABSTRACT

We review feasibility studies, technological developments and astrophysical prospects for Laue lenses devoted to unprecedented hard X-/gamma-ray astronomy observations.

## 1. INTRODUCTION

Hard X-/soft gamma-ray astronomy is a crucial window for the study of the most energetic and violent events in the Universe. With the ESA INTEGRAL observatory,<sup>1</sup> and the NASA *Swift* satellite,<sup>2</sup> unprecedented sky surveys in the band beyond 20 keV are being performed.<sup>3,4</sup> As a consequence, hundreds of celestial sources have already been discovered, new classes of Galactic sources are identified, an unprecedented overview of the extragalactic sky is available, evidence of extended matter-antimatter annihilation emission from our Galactic center<sup>5</sup> and of Galactic nucleosynthesis processes have been also reported.<sup>5,6</sup> However, in order to take full advantage of the extraordinary potential of soft gamma-ray astronomy, a new generation of telescopes is needed. The current generation has relied on the use direct-viewing detectors with mechanical collimators (e.g., BeppoSAX/PDS, Ref. 7) and, in some cases, with modulating aperture systems, like coded masks (e.g., INTEGRAL/IBIS, Ref. 8). These telescopes are penalized by their modest sensitivities, that improve at best as the square root of the detector surface. The only solution to the limitations of the current generation of gamma-ray instruments is the use of a focusing optics. Either to study the continuum emission or to study the nuclear line emission from celestial sources, Laue lenses, based on diffraction from crystals in transmission configuration, are particularly suited to focus photons in the hard X-/soft gamma-ray ( $< 1$  MeV) domain.

With these lenses, we expect a big leap in both flux sensitivity and angular resolution. As far as the sensitivity is concerned, the expected increase is by a factor of at least 10–100 with respect to the best non-focusing instruments of the current generation, either coded masks or not (e.g., INTEGRAL/IBIS, Ref. 8; BeppoSAX/PDS, Ref. 7). Concerning the angular resolution, the increase is expected to be more than a factor 10 (from  $\sim 15$  arcmin of the mask telescopes like INTEGRAL IBIS to less than 1 arcmin).

The expected astrophysical issues that are expected to be solved with the advent of these telescopes are many and of fundamental importance. A thorough discussion of the science case has been carried out in the context of the mission proposal *Gamma Ray Imager* (GRI), submitted to ESA in response to the first AO of the 'Cosmic Vision 2015–2025' plan,<sup>9</sup> but see also Refs. 9–12. We summarize here some these issues.

- *Deep study of high energy emission physics in the presence of super-strong magnetic fields (magnetars)*

The XMM and INTEGRAL observed spectra of Soft Gamma Ray Repeaters (see, e.g., Ref. 13) and Anomalous X-ray pulsars (see, e.g., Ref. 14) leave unsolved the physical origin of the high energy component ( $> 100$  keV). A better sensitivity at  $E > 100$  keV is needed.

- *Deep study of high energy emission physics in compact Galactic objects and AGNs*

A clue about the emission region and mechanism, along with the properties of the hidden black hole, can be obtained with the measurement of the high energy cutoff and its relation with the power-law energy spectrum of the compact objects. The current observational status is far to be clear (see, e.g., Ref. 15,16).

---

Further author information: (Send correspondence to F.F.)

F.F: E-mail: frontera@fe.infn.it, Telephone: +39 0532 974 254

Much more sensitive observations are needed, for either AGNs and compact Galactic sources. In the case of blazars, the gamma-ray observations are crucial for the determination of their emission properties given that their energy emission peaks at hundreds of keV.<sup>17</sup>

- *Establishing the precise role of non-thermal mechanisms in extended objects like Galaxy Clusters*

Even if significant results show that hard tails of Galaxy Clusters (GC) are clearly demonstrated to exist,<sup>18</sup> their origin is still an open issue. Are they the result of a diffuse emission or are they due to AGNs in the GC? In the former case, which is the emission mechanism? Which is their contribution to CXB? All these questions require much more sensitive observations, like those achievable with broad band Laue lenses.

- *Origin of Cosmic hard X/soft gamma-ray diffuse background*

Currently, a combination of unobscured, Compton thin and Compton thick radio-quiet AGNs populations with different scatter in the photon index distribution and fixed high energy spectral cutoff ( $E_c$ ) are assumed in synthesis models of the Cosmic X-ray background (CXB).<sup>19</sup> Is it reasonable to assume a fixed  $E_c$ ? A photon-energy dependent contribution from radio-loud AGN to CXB, like blazars, is generally assumed. But which is their real contribution contribution is still matter of discussion. Deep spectral measurements of a significant sample of AGNs beyond 100 keV is strongly needed to solve these issues.

- *Positron astrophysics*

Positron production occurs in a variety of cosmic explosion and acceleration sites, and the observation of the characteristic 511 keV annihilation line signature provides a powerful tool to probe plasma composition, temperature, density and ionization degree. The positron annihilation signature is readily observed from the galactic bulge region yet the origin of the positrons remains mysterious. Compact objects - both galactic and extragalactic - are believed to release significant numbers of positrons leading to 511 keV gamma-ray line emission in the inevitable process of annihilation. A recent SPI/INTEGRAL all-sky map<sup>5</sup> of galactic  $e^-e^+$  annihilation radiation shows an asymmetric distribution of 511 keV emission that has been interpreted as a signature of low mass X-ray binaries with strong emission at photon energies  $>20$  keV (hard LMXBs). A claim for an annihilation line from a compact source (Nova Muscae) was reported in the 90s<sup>20</sup> but was never confirmed. Much more sensitive observations are urgently needed to study the annihilation line origin, sources and their nature.

- *Physics of the supernova explosions*

Type Ia supernovae (SN Ia) are major contributors to the production of heavy elements and hence a critical component for the understanding of life cycles of matter in the Universe and the chemical evolution of galaxies. Because Laue lens telescopes allow the direct observation of radioactive isotopes that power the observable light curves and spectra, gamma-ray observations of SNe Ia that can be performed with this type of instrument are in a position to make a breakthrough on the detailed physical understanding of SNe Ia, important for its own sake, and also necessary to constrain systematic errors when using high- $z$  SNe Ia to determine cosmological parameters.

High resolution gamma-ray spectroscopy provides a key route to answering these questions by studying the conditions in which the thermonuclear explosion starts and propagates. A sensitivity of  $10^{-6}$  photons  $\text{cm}^{-2} \text{s}^{-1}$  to broadened gamma-ray lines allows observations of supernovae out to distances of 50–100 Mpc. Within this distance it is expected that there will always be a type Ia SN in the phase of gamma-ray line emission, starting shortly after explosion, and lasting several months.

In this paper, we review the physical principles of the Laue lenses, their geometry, their optimization criteria, their optical properties, the current development status and the prospects for future missions for gamma-ray astronomy.

## 2. LAUE LENS CONCEPT

Diffraction lenses use the interference between the periodic nature of light and a periodic structure such as the matter in a crystal. In a Laue lens, the photons pass through the full crystal, using its entire volume for

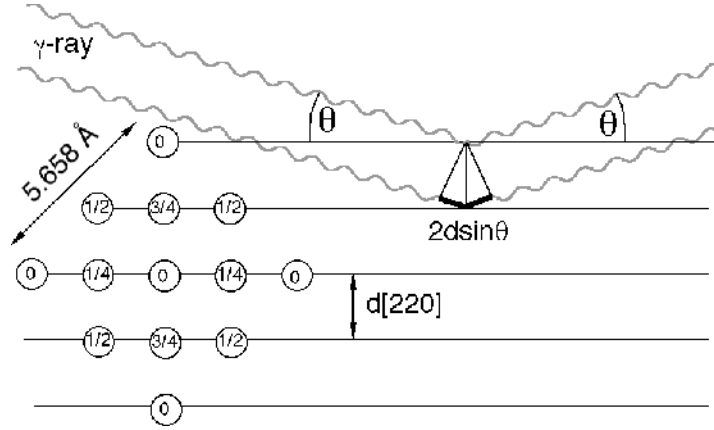


Figure 1. The Bragg condition for constructive interference of a gamma-ray photon with the atoms of a given crystalline plane (e.g. Germanium [220] planes). In the figure we assume a Germanium crystal that has a cubic structure with a side length of 5.658 Å.

interacting coherently. In order to be diffracted, an incoming gamma-ray must satisfy the Bragg-condition, relating the spacing of atomic planes  $d_{hkl}$  with the energy of incident photons  $E$  and with the angle of incidence  $\theta_B$  with respect to the chosen set of planes ( $hkl$ ) \*:

$$2d_{hkl} \sin \theta_B = n \frac{hc}{E} \quad (1)$$

where  $d_{hkl}$  (in Å) is the spacing between crystal planes ( $hkl$ ),  $n$  is the diffraction order,  $hc = 12.4 \text{ keV} \cdot \text{Å}$  and  $E$  is the energy of the gamma-ray photon. An elementary illustration of the Bragg condition is given in Fig. 1, where it is assumed that the incident waves are reflected by the parallel planes of the atoms in the crystal.

A Laue lens is made of a large number of crystals that are disposed such that they will concentrate the incident radiation onto a common focal spot. A convenient way to visualize the geometry of a crystal lens is to consider it as a spherical cup covered with crystal tiles having their diffracting planes perpendicular to the sphere (see Fig. 2). The focal spot is on the symmetry axis at a distance  $f = R/2$  from the cup, with  $R$  being the radius of the sphere of which the spherical cup is a part;  $f$  is called *focal length*. Eq. 1 requires each crystal to be oriented so that the angle between the incident beam and the crystalline planes is the Bragg angle  $\theta_B$ .

From the Bragg equation, at the first diffraction order ( $n = 1$ ), it can be seen that the incident photons on a given crystal at distance  $r$  ( $r_{min} \leq r \leq r_{max}$ ) can be reflected in the lens focus if their energy  $E$  is given by

$$E = \frac{hc}{2d_{hkl}} \sin \left[ \frac{1}{2} \arctan \left( \frac{f}{r} \right) \right] \approx \frac{hc f}{d_{hkl} r} \quad (2)$$

where the approximated expression is valid for gamma-ray lenses, given the small diffraction angles involved.

Viceversa, the lens radius  $r$  (see Fig. 2) at which the photon energy  $E$  is reflected in the focus is given by

$$r = f \tan[2\theta_B] = f \tan \left[ 2 \arcsin \left( \frac{hc}{2Ed_{hkl}} \right) \right] \approx \frac{hc f}{d_{hkl} E} \quad (3)$$

---

\*The indices  $h, k, l$ , known as *Miller indices*, are defined as the reciprocals of the fractional intercepts which the plane makes with the crystallographic axes. For example, if the Miller indices of a plane are ( $hkl$ ), written in parentheses, then the plane makes fractional intercepts of  $1/h, 1/k, 1/l$  with the axes, and, if the axial length are  $a, b, c$ , the plane makes actual intercepts of  $a/h, b/k, c/l$ . If a plane is parallel to a given axis, its fractional intercept on that axis is taken as infinity and the corresponding Miller index is zero. If the Miller indices [ $hkl$ ] are shown in square brackets, they give the direction of the plane with the same indices.

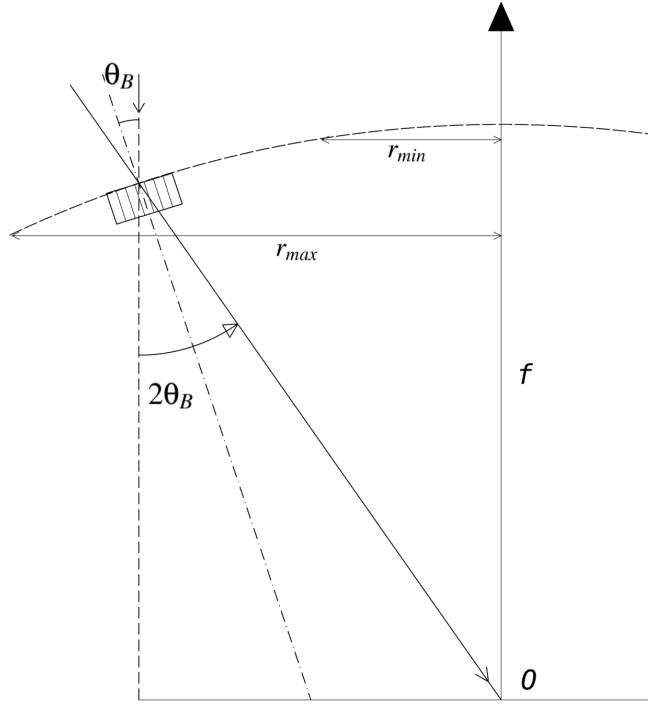


Figure 2. Geometry of a Laue lens

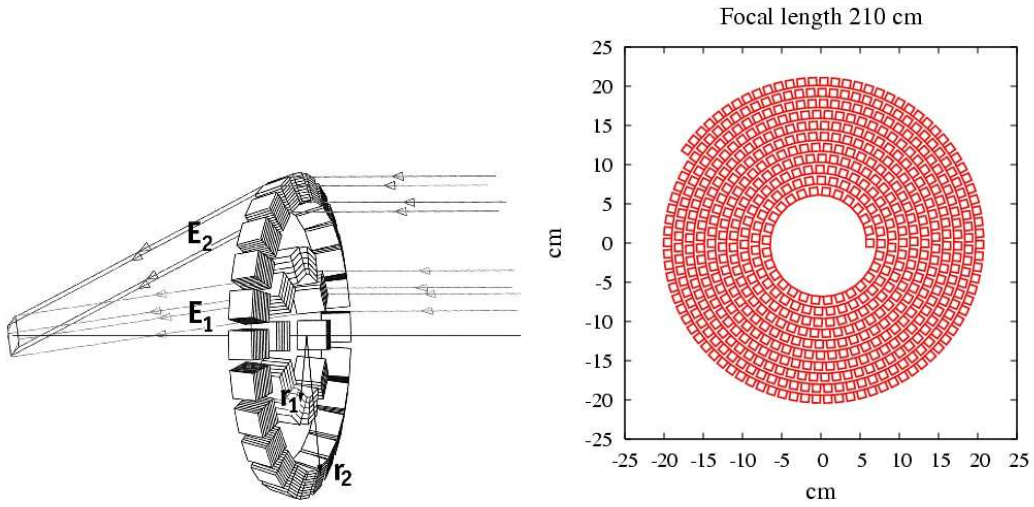


Figure 3. The basic design of a crystal diffraction lens in Laue geometry. *Left*: concentric rings of a given radius  $r$  concentrating a constant energy  $E$ . *Right*: crystal tiles disposed along an Archimedes' spiral results in a continuously varying energy  $E$ . Given the footprint of the crystals, the image in the focal plane has as minimum size that of the crystal size.

The rotation around the lens optical axis at constant  $r$  results in concentric rings of crystals (see left panel of Fig. 3), while a uniformly changing value of  $r$  gives rise to an Archimedes spiral (right panel of Fig. 3). Assuming that the chosen diffracting planes ( $hkl$ ) of all the lens crystals are the same, in the first case (constant  $r$ ) the energy of the diffracted photon will be centered on  $E$  for all the crystals in the ring, while in the second case (Archimedes spiral), the reflected energy  $E$  will continuously vary from one crystal to the other.

## 2.1 Energy bandpass

Any Laue lens, broad- or narrow-band (see below), will diffract photons over a certain energy passband ( $E_{min}, E_{max}$ ). From eq. 2, at first order diffraction (the most efficient), it results that

$$E_{min} \approx \frac{hcf}{d_{hkl} r_{max}} \quad (4)$$

$$E_{max} \approx \frac{hcf}{d_{hkl} r_{min}}. \quad (5)$$

Given that the lens passband has to be covered with the highest effective area <sup>†</sup> and in a smooth manner, the energy band of the photons reflected by contiguous crystal rings or, in the case of the Archimedes structure of a lens, by contiguous crystals, have to superimpose with each other. Since the acceptance angle  $\Delta\theta$  (known as *Darwin width*) of perfect crystals is extremely narrow (fractions of arcsec to a few arcsec, see Ref. 21) such materials are not suitable for astrophysical Laue lenses. In order to increase the energy bandpass of individual crystals one uses mosaic crystals or curved crystals (see following section). The mosaic width, or mosaicity, of the crystals governs the flux throughput, the angular resolution and the energy bandpass of the crystal lens. The diffracted flux from a continuum source increases with increasing mosaic width of the crystal. For a crystal lens telescope, crystals with mosaic widths ranging from a few tens of arc seconds to a few arc minutes are of interest.

The bandwidth of a lens for an on-axis source is determined by the mosaicity of the individual crystals and the accuracy of the alignment of the crystals. By forming the derivative of the Bragg relation in the small angle approximation ( $2d\theta_B \approx hc/E$ ),

$$\Delta\theta_B/\theta_B = \Delta E/E, \quad (6)$$

where  $\Delta\theta$  is the mosaic width of the crystal; the energy bandpass  $\Delta E$  of the crystal becomes

$$\Delta E = \frac{2d \cdot E^2 \cdot \Delta\theta_B}{nhc}. \quad (7)$$

It is worth pointing out that, whereas the energy bandpass of a crystal lens grows with the square of energy, the Doppler broadening of the astrophysical lines (e.g. in SN ejecta) increases linearly with energy for a given expansion velocity.

## 3. CRYSTAL STRUCTURE

Either mosaic crystals and/or curved crystals are suitable to be used for a Laue lens. We discuss the properties of both of them and their reflectivity.

### 3.1 Mosaic crystals

Mosaic crystals are made of many microscopic perfect crystals (*crystallites*) with their lattice planes slightly misaligned with each other around a mean direction, corresponding to the mean lattice planes (*hkl*) chosen for diffraction. In the lens configuration assumed, the mean lattice plane is normal to the mosaic crystal surface. The distribution function of the crystallite misalignments from the mean direction can be approximated by a Gaussian function:

$$W(\delta) = \frac{1}{\sqrt{2\pi}\eta} \exp\left(-\frac{\delta^2}{2\eta^2}\right), \quad (8)$$

where  $\delta$  is the magnitude of the angular deviation from the mean, while  $\beta = 2.35\eta$  is the fwhm of the mosaic spread (called *mosaicity*).

---

<sup>†</sup>The effective area at energy  $E$  is defined as the geometrical area of the lens projected in the focal plane times the reflection efficiency at energy  $E$ .

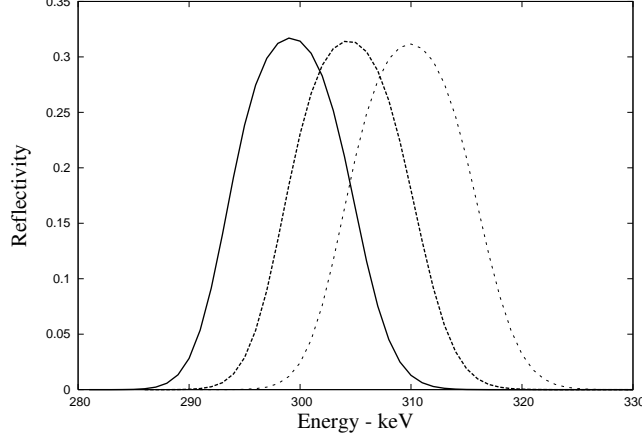


Figure 4. An example of the reflectivity profile of three contiguous crystals with a mosaicity of 1.5 arcmin along an Archimedes' spiral. Reprinted from Ref. 22.

For the Laue geometry and diffracting planes perpendicular to the cross section of the crystal tile (see, e. g., Fig. 2), the crystal reflectivity  $R(\Delta, E)$  is given by Ref. 21:

$$R(\delta, E) = \frac{I_d(\delta, E)}{I_0} = \sinh(\sigma T) \exp \left[ -(\mu + \gamma_0 \sigma) \frac{T}{\gamma_0} \right] = \frac{1}{2} (1 - e^{-2\sigma T}) e^{-\mu \frac{T}{\gamma_0}}, \quad (9)$$

where  $I_0$  is the intensity of the incident beam,  $\mu$  is the absorption coefficient per unit of length corresponding to that energy,  $\gamma_0$  is the cosine of the angle between the direction of the photons and the normal to the surface,  $T$  is the thickness of the mosaic crystal and  $\sigma$  is:

$$\sigma = \sigma(E, \delta) = W(\delta) Q(E) f(A), \quad (10)$$

where

$$Q(E) = \left| \frac{r_e^2 F_{hkl}}{V} \right|^2 \lambda^3 \frac{1 + \cos^2(2\theta_B)}{2 \sin 2\theta_B}, \quad (11)$$

in which  $r_e$  is the classical electron radius,  $F_{hkl}$  is the structure factor, inclusive of the temperature effect (Debye-Waller's factor),  $V$  is the volume of the crystal unit cell,  $\lambda$  is the radiation wavelength and  $\theta_B$  is the Bragg angle for that particular energy, while  $f(A)$  is given by:

$$f(A) = \frac{B_0(2A) + |\cos 2\theta_B| B_0(2A |\cos 2\theta_B|)}{2A(1 + \cos^2 \theta_B)} \quad (12)$$

where  $B_0$  is the Bessel function of zero order integrated between 0 and  $2A$ , with  $A$  defined as follows:

$$A = \frac{\pi t_0}{\Lambda_0 \cos \theta_B}, \quad (13)$$

in which  $t_0$  is the crystallite thickness, and  $\Lambda_0$  (*extinction length*) is defined for the symmetrical Laue case (see e.g. ref. 23) as:

$$\Lambda_0 = \frac{\pi V_c \cos \theta_B}{r_e \lambda |F_{hkl}| (1 + |\cos 2\theta_B|)}, \quad (14)$$

In general  $f(A) < 1$  and converges to 1 if  $t_0 \ll \Lambda_0$ . In this case we get the highest reflectivity.

The quantity  $\gamma_0 \sigma$  is known as *secondary extinction* coefficient and  $T/\gamma_0$  is the distance travelled by the direct beam inside the crystal.

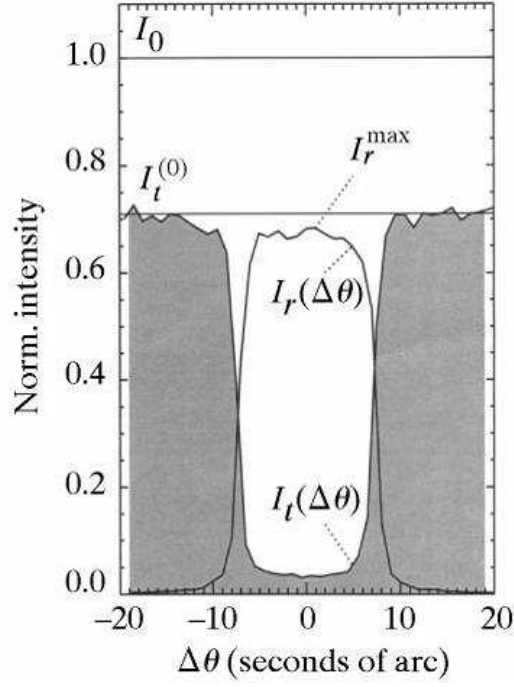


Figure 5. Reflectivity profile of a curved crystal as a function of the rocking angle  $\Delta\theta$ .  $I_0$  represents the incident intensity,  $I_t(\Delta\theta)$  the transmitted intensity and  $I_r(\Delta\theta)$  the reflected intensity. Reprinted from Ref. 25.

### 3.2 Curved crystals

Similarly to mosaic crystals, curved crystals have an angular dispersion of the lattice planes and thus a much larger energy passband (see Eq. 7) than perfect crystals. The properties of these crystals and the methods to get them are discussed by Ref. 24. Here we summarize the their reflection reflection properties.

The most recent theory of the radiation diffraction in transmission geometry for such crystals, in the case of a large and homogeneous curvature, is now well fixed and compared with the experimental results (see, e.g., Ref. 25,26). In this theory, the distortion of diffracting planes is described by the strain gradient  $\beta$ , that, in the case of a uniform curvature, is given by:

$$\beta = \frac{\Omega}{T_0(\delta/2)} \quad (15)$$

where  $\Omega$  being the fwhm of the angular distribution of planes (we will call *mosaicity* as well for similarity with mosaic crystals),  $T_0$  the thickness of the crystal and  $\delta$  the Darwin width.

When the strain gradient  $|\beta|$  becomes larger than the critical value  $\beta_c = \pi/(2\Lambda_0)$ , it has been shown that, for a uniform curvature of planes, the peak reflectivity  $R^{max}$  of a curved crystal is given by:

$$R^{peak}(c_p, E) = \frac{I_r^{peak}(c_p, E)}{I_0} = \left(1 - e^{-\frac{\pi^2 d_{hkl}}{c_p \Lambda_0^2}}\right) e^{-\frac{\mu \Omega}{c_p \cos \theta_B}}. \quad (16)$$

where  $I_r^{peak}$  is the reflected peak intensity,  $c_p = \Omega/T_0$  is the curvature of the lattice planes assumed to be uniform across the crystal thickness, and the extinction length  $\Lambda_0 = \Lambda_0(E)$  is given by the Eq. 14. The reflected intensity profile  $I_r(c_p, E)$  is that of a perfect crystal with the Darwin width replaced with  $\Omega$ . This profile is shown in Fig. 5.

From the last equation, it can be shown that the highest peak reflectivity is obtained for a curvature of the lattice planes given by:

$$c_p^{opt} = \frac{M}{\ln\left(1 + \frac{M}{N}\right)}. \quad (17)$$

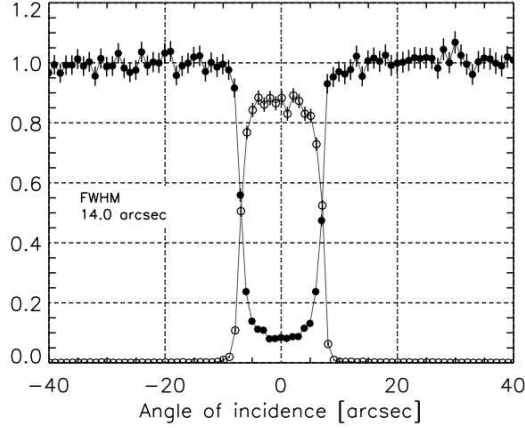


Figure 6. Measured rocking curve, in transmission geometry at 150 keV, of a Si (111) crystal curved at the University of Ferrara (see text). Reprinted from Ref. 28.

where  $M = \frac{\pi^2 d_{hkl}}{\Lambda_0^2}$  and  $N = \frac{\mu \Omega}{\cos \theta_B}$ .

### 3.3 Mosaic crystals vs. curved crystals

Both mosaic crystals and curved crystals can be used for a Laue lens, if they can be produced with the needed angular spread. However, in principle, curved crystals can reach a higher efficiency than mosaic crystals. Indeed, while the diffraction efficiency of mosaic crystals is limited to 50%, that of curved crystals can reach 100%. Another advantage of curved crystals is that the diffraction profile of a curved crystal is rectangular with width related to  $\Omega$ , while that of mosaic crystals is Gaussian with fwhm equal to the mosaicity  $\beta$ . Thus curved crystals, given that do not have the Gaussian tails, better concentrate the gamma-rays. This better performance of the curved crystals with respect to the mosaic crystals for Laue lenses is widely discussed in Ref. 27.

Curved crystals can be obtained in various ways.<sup>24</sup> The most feasible techniques to be used for Laue lenses include the bending of an elastically perfect crystal (technique commonly adopted in synchrotron radiation facilities), the deposition of a coating on a wafer, by growing a two-component crystal whose composition varies along the crystal growth axis, the grooving of one face of a wafer. The last one is being developed at the University of Ferrara (V. Guidi, private communication) with very satisfactory results (see Fig. 6). Also the deposition of a coating on a wafer is being tested at the same University.

## 4. OPTIMIZATION OF A LAUE LENS

The free parameters of a Laue lens are the crystal properties (materials, lattice planes for diffraction, micro-crystal thickness in the case of mosaic crystals, crystal thickness, mosaicity), the lens geometry (ring-like or Archimedes' spiral), its focal length and its nominal energy passband. Many optimization studies of these parameters have been performed and tested.<sup>24, 29–31</sup>

### 4.1 Crystal material

Independently of the crystal structure (mosaic or curved), in order to optimize the crystal reflectivity it is important to maximize Eq. 11 that is, the integrated crystal reflectivity per unit volume, whose normalization is the ratio  $|F_{hkl}/V|^2$  between the structure factor of the chosen lattice planes  $F_{hkl}$  and the volume  $V$  of the unit cell. The inverse of  $V$ , i.e. the number density of unit cells, of all elements is shown in Fig. 7. As can be seen, for single-element materials, broad density peaks are apparent in correspondence of the atomic numbers 5, 13, 28, 45, and 78. Common hard materials like Al ( $Z = 13$ ), Si ( $Z = 14$ ), Ni ( $Z = 28$ ), Cu ( $Z = 29$ ), Zn ( $Z = 30$ ), Ge ( $Z = 32$ ), Mo ( $Z = 42$ ), Rh ( $Z = 45$ ), Ag ( $Z = 47$ ), Ta ( $Z = 73$ ), W ( $Z = 74$ ), Au ( $Z = 79$ ) are good candidates to be used for Laue lenses and should be preferred to other elements if they are available with the requested properties. The peak reflectivity versus energy of few single-element mosaic crystal materials is shown in Fig. 8.



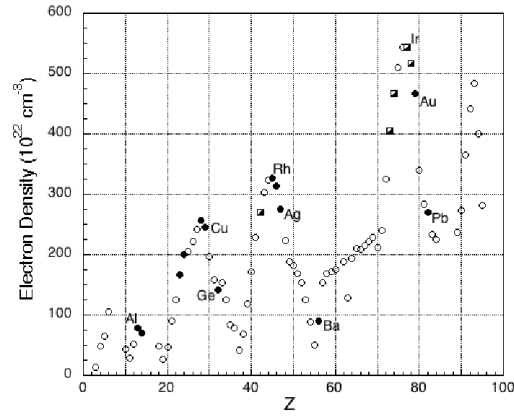


Figure 7. Density of a crystal unit cell versus element atomic number. Reprinted from Ref. 24.

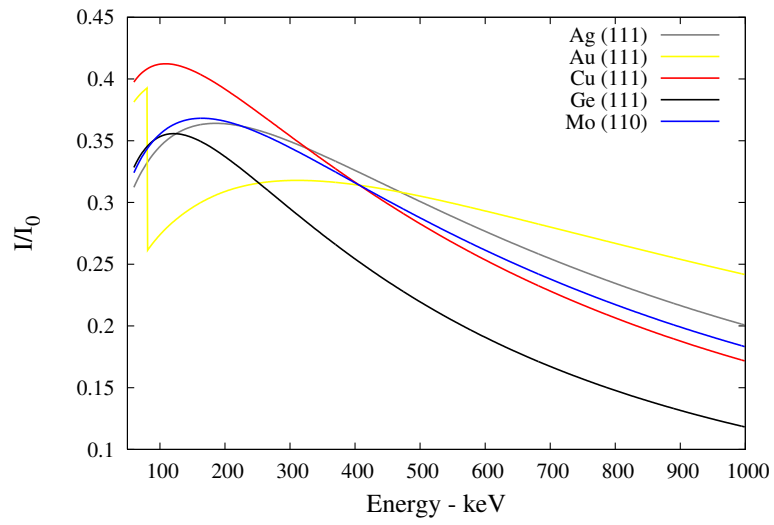


Figure 8. Peak reflectivity of 5 candidate crystal materials. The Miller indices used give the highest reflectivity. A mosaicity of 40 arcsec is assumed. The thickness has been optimized. The production technology of mosaic crystals with the required spread is already mature for for Ge and Cu.

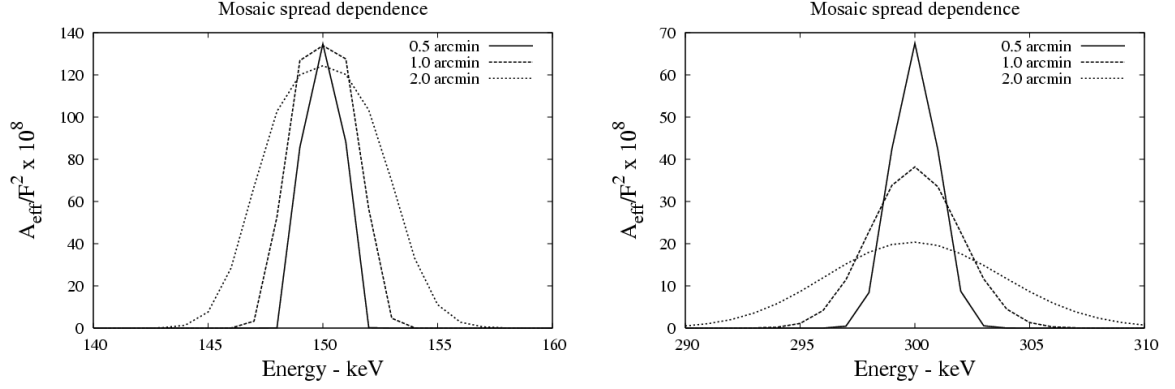


Figure 9. Normalized effective area for different values of the mosaicity. *Left*: First diffraction order; *Right*: second diffraction order. Reprinted from Ref. 31.

For double-elements crystal materials, their choice can be only based on their feasibility. Several two-elements crystals are already available, like GaAs, InAs, CdTe, CaF<sub>2</sub>, being developed for other applications. With some improvements they could be used for Laue lenses (see discussion in Ref. 24).

Clearly the best lattice planes are those that optimize the structure factor  $|F_{hkl}|$ , under the condition that the corresponding  $d_{hkl}$  is consistent with lens constraints, like energy passband, lens size and focal length (see below).

#### 4.2 Crystallite size and angular distribution of the mosaic crystals

From the reflectivity equation (Eq. 9), it results that the crystallite thickness  $t_0$  has an important role for the reflectivity optimization. For fixed values of the mosaicity and crystal thickness, the highest reflectivity is obtained for a crystallite thickness that satisfy the condition  $t_0 \ll \Lambda_0$ . In general, that implies a thickness of the order of 1  $\mu\text{m}$ .

Unfortunately this condition is still not always satisfied. From extended tests performed on Cu(111) supplied by ILL,<sup>32</sup> it results that the condition above is satisfied in single points,<sup>22</sup> but not when the entire crystal cross section is irradiated (values even higher than 100  $\mu\text{m}$  have been found<sup>24</sup>). In addition, in Ref. 24 it is found that  $t_0$  is energy dependent, which seems an unphysical result (see discussion therein).

The crystal mosaicity is another among the most crucial parameters for the optimization of the lens performance. It can be seen<sup>11,29-31</sup> that, even if a higher mosaicity gives a larger lens effective area (see Fig. 9), a higher spread also produces a larger defocusing of the reflected photons in the focal plane and thus a lower lens sensitivity.

This can be seen by introducing the focusing factor  $G(E)$  of a Laue lens:

$$G(E) = f_{ph} \frac{A_{eff}(E)}{A_d} \quad (18)$$

in which  $A_{eff}(E)$  is the effective area of the lens and  $A_d$  is the area of the focal spot which contains a fraction  $f_{ph}$  of photons reflected by the lens.

In alternative to the focusing factor  $G(E)$ , and related to it, some authors introduce the so-called *factor of merit*  $FM(E)$ , defined as

$$FM(E) = f_{ph} \frac{A_{eff}(E)}{r_d} \quad (19)$$

where  $r_d$  is the radius of the area  $A_d$  of the focal spot assumed to be circular.

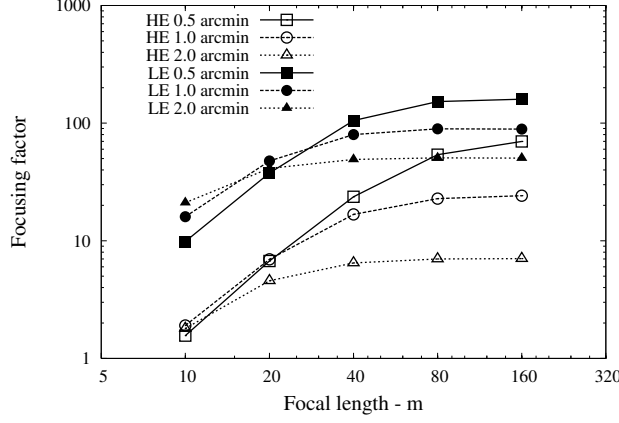


Figure 10. Dependence of the focusing factor  $G$  on the focal length  $F$  for three different values of the mosaicity in two different energy bands: 90–110 keV (LE) and 450–550 keV (HE). Reprinted from Ref. 11.

It results that  $G(E)$  is inversely proportional to the lens sensitivity for continuum emission:

$$I_{min}(E) = \frac{n_{\sigma}}{\eta_d G} \sqrt{\frac{2B}{A_d \Delta T \Delta E}} \quad (20)$$

where  $I_{min}$  (photons  $\text{cm}^{-2} \text{s}^{-1} \text{keV}^{-1}$ ) is the the minimum detectable intensity in the interval  $\Delta E$  around  $E$ ,  $n_{\sigma}$  is the significance level of the signal (typically  $n_{\sigma} = 3-5$ ),  $B$  is the focal plane detector background intensity (counts  $\text{cm}^{-2} \text{s}^{-1} \text{keV}^{-1}$ ),  $\Delta T$  is exposure time to a celestial source, and  $\eta_d$  is the focal plane detector efficiency at energy  $E$ . Figure 10 shows the dependence of  $G$  in two different energy bands on focal length for different values of the mosaicity.

As it can be seen, in spite that a higher spread gives a higher effective area, a lower spread gives a higher  $G$  and thus a higher lens sensitivity. This effect is small at low focal lengths (10–20 m), but it becomes very significant at high focal length ( $>30$  m), specially at high energies ( $\sim 500$  keV).

### 4.3 Crystal thickness

The crystal thickness is another crucial parameter for the reflectivity optimization of a mosaic crystal. The best crystal thickness is given by

$$T_{best} = \frac{1}{2\sigma} \ln \left( 1 + \frac{2\sigma\gamma_0}{\mu} \right) \quad (21)$$

in the case of a mosaic crystal, and it is given by

$$T_{best} = \frac{\Omega \ln \left( 1 + \frac{M}{N} \right)}{M}. \quad (22)$$

in the case of a curved crystal, where the involved quantities are defined in the sections above.

In the case of a mosaic crystal, the best crystal thickness for various materials is shown in Fig. 11.

As can be seen, the best crystal thickness depends on the absorption coefficient  $\mu$ . A high absorption coefficient implies a low crystal thickness for the reflectivity optimization.

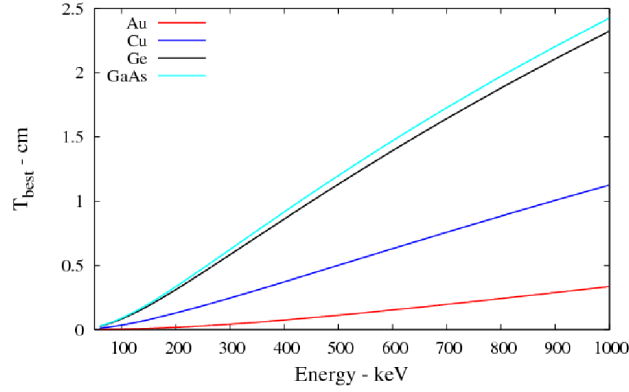


Figure 11. The best crystal thickness that maximize the crystal reflectivity, for various materials. The mosaicity assumed is 1 arcmin, the crystallite thickness is 1  $\mu\text{m}$ , and the crystal plane chosen for all of them is (111).

#### 4.4 Focal length

The focal length has a key importance in the case of Laue lenses, more than its role in the case of focusing telescopes. Indeed, given that the energy passband of a single crystal is very narrow (see e.g., Fig. 4), from the nominal energy passband ( $E_{min}$ ,  $E_{max}$ ) (see eqs. 4 and 5), at first order diffraction, the inner and outer radii of a lens ( $r_{min}$ ,  $r_{max}$ ), needed to get the lens passband linearly, depends on  $f$ :

$$r_{min} \approx \frac{hcf}{d_{hkl} E_{max}} \quad (23)$$

$$r_{max} \approx \frac{hcf}{d_{hkl} E_{min}}. \quad (24)$$

Thus  $f$  is crucial to extend the lens passband. Given that high energy photons are focused by the innermost part of the lens, the lens inner area can be increased only increasing the focal length (the lens area approximately increases with  $f^2$ ).

A gamma-ray lens with a broad continuum coverage from 300 keV to 1.5 MeV was proposed in the 90's by N. Lund.<sup>33</sup> He assumed mosaic crystals of Copper and Gold. In order to achieve a significant effective area at high energies (350 cm<sup>2</sup> at 300 keV and 25 cm<sup>2</sup> at 1.3 MeV), the focal length requested was 60 m.

#### 4.5 Broad vs. narrow bandpass Laue lenses

For the lens optimization, the selection criteria of the crystal material and lattice planes can change depending on the requested lens passband. Two lens classes can be identified, *broad* bandpass Laue lenses and *narrow* bandpass Laue lenses, the former to cover a broad energy band (e.g., 100-600 keV) for the study of continuum source spectra, the latter to achieve an optimal sensitivity in a relatively narrow energy band (e.g., 800-900 keV) for gamma-ray line spectroscopy studies.

These two classes of lenses require different criteria in the crystal choice and disposition in the lens for its optimization.

##### 4.5.1 Narrow bandpass Laue lenses

Assuming a ring-like geometry, these lenses use a different crystalline plane ( $hkl$ ) for every ring in order to diffract photons in only one energy band centered, e.g., on an energy  $E_0$ . For this energy centroid, a ring with a radius  $r_1 > r_0$ , must reflect at an angle  $\theta_{B1} > \theta_{B0}$  to concentrate the incident beam energy at a given focal distance. According to the Bragg diffraction law, this is only possible if the crystalline plane spacing  $d_1$  is smaller than  $d_0$  or if a higher order is used. The ring radii are determined by the Miller indices ( $hkl$ ). From eq. 3, for

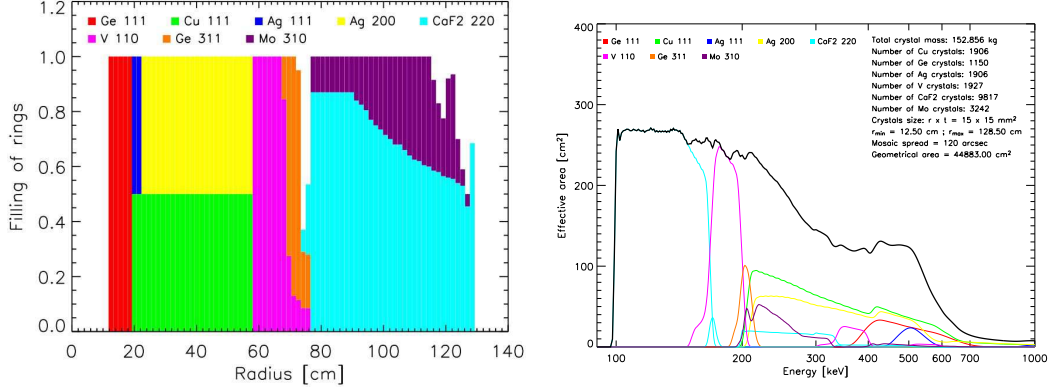


Figure 12. *Left*: Distribution of various mosaic crystals and chosen lattice planes in an example of lens with passband from 100 to 600 keV and 20 m focal length studied by Barriere et al.<sup>28</sup> *Right*: Effective area of the studied lens. Colors show the contribution of each material.

materials with a cubic structure (e.g., the face-centered cubic cell of copper, germanium or silicon), for which  $d_{hkl}$  is inversely proportional to  $\sqrt{h^2 + k^2 + l^2}$ , the ring radii are proportional to this quantity.

As the diffraction efficiency decreases with increasing diffraction order  $n$ , a crystal in an exterior ring will add less efficient area to the lens than a crystal on an inner ring. However, since the number of crystals increases with the ring-radius, all rings will usually contribute about the same amount of efficient area to the lens. Using larger and larger Bragg angles with increasing ring radius allows the instrument to be relatively compact, featuring a shorter focal length than requested if the above criterion would not be adopted. An example of a narrow bandpass Laue lens, the balloon telescope CLAIRE, will be discussed below.

#### 4.5.2 Broad bandpass Laue lenses

These lenses use the best combination of crystalline planes to cover in the most efficient way the lens passband. Lowest order planes, e.g. (111), are preferred because we can exploit, in addition to their optimum diffraction efficiency, also the higher order diffraction of the same planes. The principle used for covering a broad energy band is the following. In the simple assumption that a single crystal material and crystal plane ( $hkl$ ) are used, assuming a ring-like geometry of the lens, different concentric rings focus slightly different energies because of the varying Bragg angle, and thus with several rings a broad energy band can be covered with the first order diffraction (lens nominal energy passband). But, in addition to the first order diffraction, higher order diffraction can be exploited that increase the effective area at higher energies also extending the passband.

An example of distribution of various crystals and lattice planes in different rings for a broad bandpass lens (100–600 keV) made of mosaic crystals with 20 m focal length, studied by Ref. 28, is shown in Fig. 12.

Diffraction lenses with broad energy bandpass were also developed and tested for low energy X-rays since the sixties (e.g. Lindquist and Webber<sup>34</sup>). Today, photons up to 80 keV can be efficiently focused thanks to the development of grazing incidence and multilayers mirrors (see other papers in this issue). Above this upper threshold, the development of Laue lens telescopes become crucial for the photon focusing.

### 5. OPTICAL PROPERTIES OF A LENS

The optical properties of a lens, for either on-axis and off-axis incident photons, have been investigated by means of Monte Carlo (MC) simulations.<sup>11,31</sup> For flat crystal tiles, the Point Spread Function (PSF) depends on the crystal size, on their mosaicity and on the accuracy of their positioning in the lens.

In Fig. 13 we show two derived on-axis Point Spread Functions for two cases: a ring-shaped lens of 40 m focal length and a spiral-shaped lens of 6 m focal length, respectively. In the first case the lens has a 150–600 keV energy passband and a crystal tile cross section of  $10 \times 10 \text{ mm}^2$ , while in the second case it has a 70–300 keV passband and a crystal tile cross section of  $15 \times 15 \text{ mm}^2$ . In both cases it is supposed that the crystals have

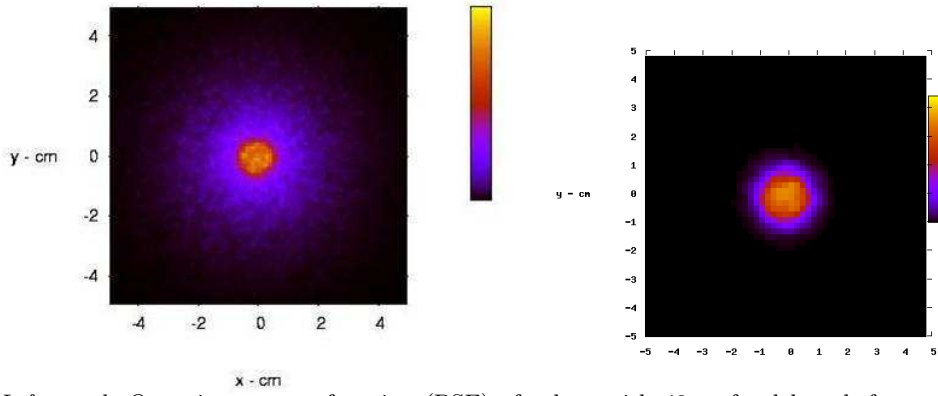


Figure 13. *Left panel:* On axis response function (PSF) of a lens with 40 m focal length for an on-axis source in the 150–600 keV energy band. *Right panel:* Point spread function of a lens with 6 m focal length for an on-axis source in the 70–300 keV energy band. See text. Reprinted from Ref. 35,36.

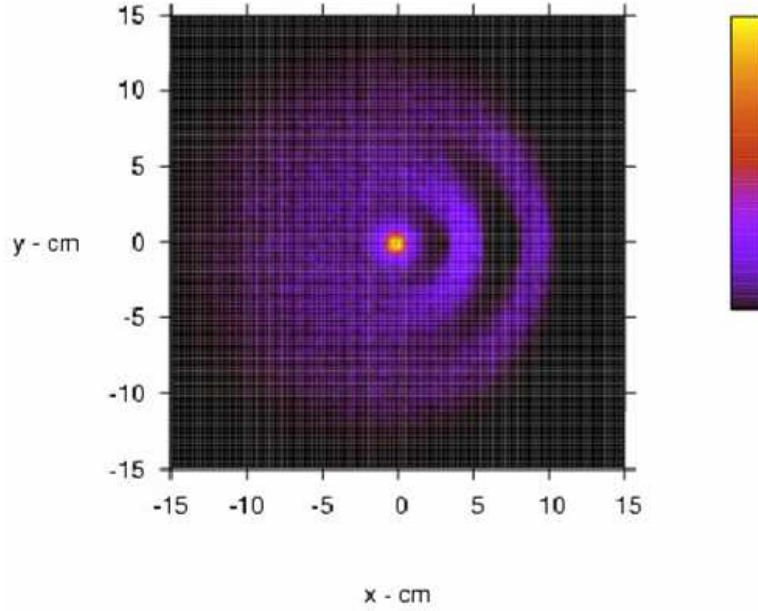


Figure 14. Off-axis expected response function (PSF) of a Laue lens with 40 m focal length. Three point sources are simulated, at 0, 2 and 4 arcmin off-axis. See text. Reprinted from Ref. 36.

a mosaic structure with 1 arcmin spread and that they are properly oriented in the lens. The 6 m focal length lens has been proposed for a balloon experiment.<sup>35</sup>

In the case of curved crystals, whose development is giving very satisfactory results (see section 3.3), the expected PSF becomes very sharp, with a great advantage in terms of angular resolution and sensitivity. Assuming a lens of 15 m focal length made of mosaic crystals with a spread of 30 arcsec, the PSF obtained in the case of  $15 \times 15 \text{ mm}^2$  flat mosaic crystals and that obtained in the case of curved crystals with a curvature radius of 30 m (2 times the focal length) are shown in Fig. 15. The difference between the two PSF is outstanding. In the case of curved crystals we expect an angular resolution of 20 arcsec and a higher sensitivity by almost a factor 10.

In Fig. 14, for flat crystal tiles of  $15 \times 15 \text{ mm}^2$ , we show the expected PSF of the 40 m focal length lens when three sources are in its Field of View (FOV), with one of the sources on-axis and the other two off-axis. As can

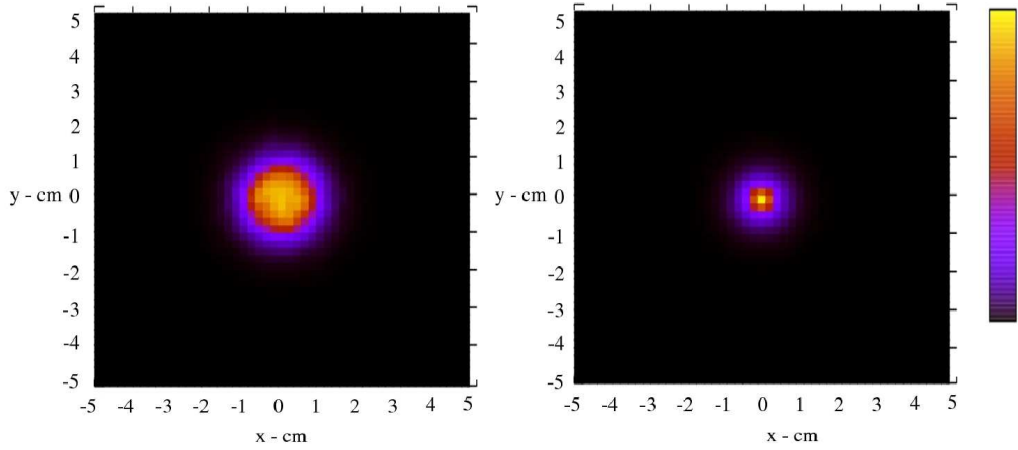


Figure 15. On axis response function (PSF) of a lens of 15 m focal length made of mosaic crystals with 30 arcsec spread, for an on-axis source. *Left panel:* Flat crystals with cross section of  $15 \times 15 \text{ mm}^2$ . *Right panel:* Curved crystals with a curvature radius of 30 m.

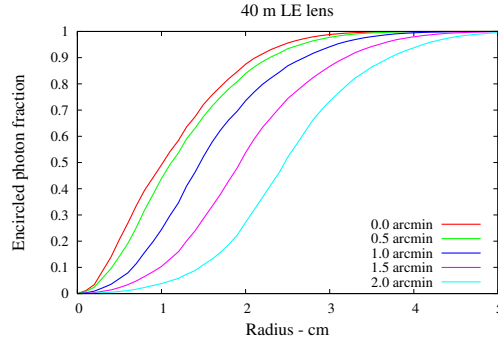


Figure 16. Cumulative distribution of photons with the distance from the lens focus, for different values of the mosaic spread, 40 m focal length lens, at about 100 keV.

be seen, in the case of off-axis sources the image has a ring shape with center in the lens focus, inner radius that increases with the offset angle, and a non uniform distribution of the reflected photons with azimuth. It is found that the integrated number of photons focused by the lens does not significantly vary from an on-axis source and to an off-axis source, but its space distribution spread over. As a consequence, the FOV of the lens is determined by the detector radius, taking into account that the focused photons from sources at increasing offset spread over an increasing area, and the lens sensitivity decreases with source offset. The azimuthal disuniformity of the PSF for off-axis sources can be usefully exploited, because it gives information on the azimuthal source direction. The angular resolution, in addition to the size of the flat crystal tiles, depends on the mosaic spread and on the misalignments of the lens crystal tiles. For the lens image shown in Fig. 14, the angular resolution is of the order of, or even better than, 1 arcmin.

Figure 16 shows the cumulative distribution of the on-axis photons with the distance from the lens focus, for different values of the mosaic spread, in the case of a 40 m focal length lens with  $15 \times 15 \text{ mm}^2$  flat crystal tile cross section. As can be seen, for a low mosaic spread, the distribution is driven by the crystal size, while for large spreads, it is mainly driven by this spread.

## 6. THE DEVELOPMENT OF LAUE LENSES

Two key issues have to be faced in order build a Laue lens:

- Development of technologies for the massive production of suitable crystals (mosaic and/or curved crystals) in a reasonable time, consistent with that of preparation of a space mission;
- Development of a technology for assembling, in an equally reasonable time, thousands of crystal tiles in a lens with the proper orientation accuracy, that largely depends on the focal length.

Laue lens developments are being carried out in different institutions. We summarize here the major results obtained in our institutes.

### 6.1 CLAIRE – a narrow bandpass Laue lens experiment

The objective of the R&D project CLAIRE<sup>37</sup> was to demonstrate that a prototype Laue lens prototype can work under space conditions, measuring its performance by observing an astrophysical target. The CLAIRE telescope was flown twice (2000, 2001) on a stratospheric balloon by the French Space Agency CNES. CLAIRE's Laue lens was further tested on a 205 m long optical bench in 2003.<sup>38</sup> The project involved research groups from CESR Toulouse, University of Birmingham, ILL Grenoble, IEEC Barcelona, and ANL Chicago. CLAIRE's *narrow bandpass* lens consisted of 556 crystals (see Table 1) mounted on the eight rings of a 45 cm diameter Titanium frame. In each ring  $i$ , the combination of the crystal plane spacing  $d_i$  and the Bragg angle  $\theta_{Bi}$  results in the concentration of 170 keV photon onto a common focal spot of 1.5 cm diameter at 279 cm behind the lens.

CLAIRE's crystals were produced by N. Abrosimov at the Institut für Kristallzüchtung (IKZ) in Berlin. The Germanium-rich  $\text{Ge}_{1-x}\text{Si}_x$  crystals ( $x \approx 0.02$ ) were grown by a modified Czochralski technique using Silicon feeding rods to replenish the loss of Si in the melt during the growth. The mosaicities of the  $\text{Ge}_{1-x}\text{Si}_x$  crystals range between roughly 30 arcsec and 2 arcmin, leading to a field of view of about 1.5 arcmin and a diffracted energy bandwidth of about 3 keV at 170 keV. A correlative study between crystal structure, mosaicity and diffraction efficiency of the CLAIRE crystals is presented in Abrosimov et al (2005).<sup>39</sup> After cutting of the crystals ingots at IKZ Berlin, most of the crystal tiles were characterized (mosaicity) at the Hard X-Ray Diffractometer of ILL Grenoble.

At CESR Toulouse, the individual crystal tiles were mounted on flexible aluminium supports, which in turn are mounted on the lens frame. The reinforced 45 cm diameter titanium frame that holds up to 576 crystals on 8 rings was designed and manufactured at the Argonne National Laboratory, Argonne, USA. The tuning of the lens consisted of tilting each crystal tile to the appropriate Bragg angle so that the diffracting energy was 170 keV for a source at infinity. Instead of directly calibrating the lens for a parallel beam of 170 keV photons, crystal tuning on the 20 m optical bench at CESR used a 150 kV X-ray generator situated on the lens optical axis at a distance of 14.16 m. At this distance, a crystal was correctly tuned (170 keV at infinity) if it diffracts 122.28 keV photons. A co-aligned mask (brass-lead sandwich) of the size of the entire lens, placed on the optical axis just in front of the lens, was used to select an individual crystal for tuning, while shielding already tuned crystals.

The resulting geometric area of the CLAIRE lens was  $511 \text{ cm}^2$ , the FOV and the bandpass were  $90''$  and  $\sim 3 \text{ keV}$ , respectively. The photons were focused onto a small  $3 \times 3$  array of high-purity Germanium detectors, housed in a single cylindrical aluminum cryostat. Each of the single Ge bars was an n-type coaxial detector with dimensions of  $1.5 \text{ cm} \times 1.5 \text{ cm} \times 4 \text{ cm}$ . Focusing onto such a small detector volume already results in very low background noise. The CLAIRE stabilization and pointing system was developed by the balloon division of the French space agency CNES.

**CLAIRE's first light :** On June 14 2001, CLAIRE was launched by the balloon division of French Space Agency CNES from its base at Gap-Tallard in the French Alps. The astrophysical target was the Crab Nebula. (While nuclear lines are the perfect astrophysical targets for narrow bandpass Laue lenses, the balloon test flight ironically required the observation of a continuum spectrum.) With a mere 72 minutes of the flight having satisfactory pointing, CLAIRE nevertheless collected 33 photons from the Crab Nebula. This  $3 \sigma$  detection has been validated by ground tests led at distances of 14.16 m, 22.52 m (CESR optical bench) and 205 m (long



ring	reflection [hkl]	d [hkl] [Å]	size [mm]	number of crystals	radius [cm]	Bragg angle at 170 keV
0	111	3.27	10 x 10	28	6.17	0.64
1	220	2.00	10 x 10	52	10.08	1.04
2	311	1.71	10 x 10	56	11.82	1.22
3	400	1.41	10 x 10	72	14.26	1.48
4	331	1.30	10 x 7	80	15.62	1.61
5	422	1.15	10 x 10	96	17.47	1.81
6	333	1.09	10 x 7	96	18.82	1.92
7	440	1	10 x 10	104	20.17	2.09

Table 1. The crystalline plane, the crystal size, the number of crystals per ring as well as the ring radius and the Bragg angle at 170 keV are listed for each ring of the prototype crystal lens.

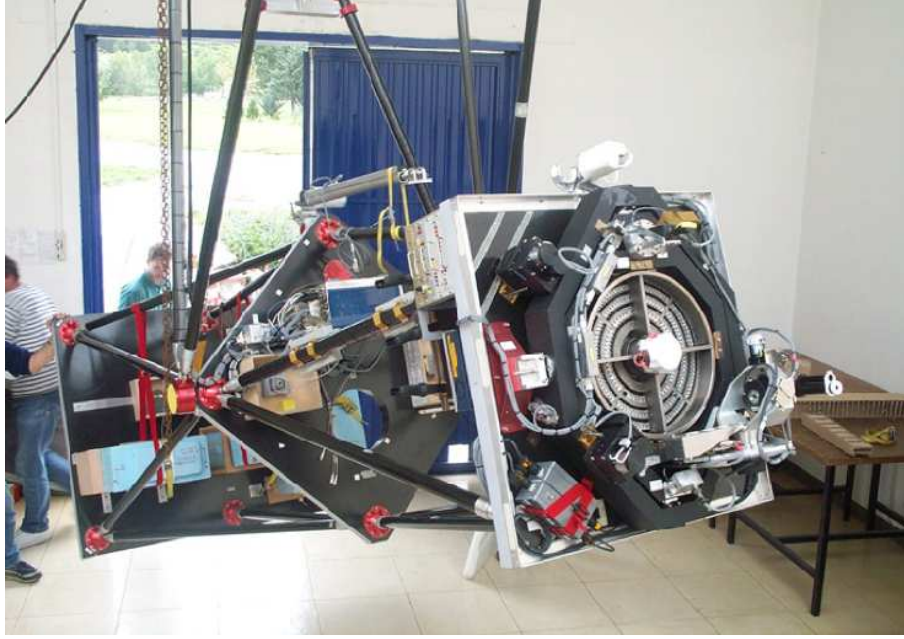


Figure 17. The CLAIRE telescope at Gap during the 2001 balloon campaign. On the first platform, the gamma-ray lens in its two-axes gimbal.

distance test, Ordís, Catalonia). Figure 18 shows the recorded spectra for these experiments. The energies of the centroids are in very good agreement with theory, slight departures from theoretical values (less than 0.5 keV) being the consequence of the incident spectrum shape and/or the detector calibration drifts. The measured peak efficiencies of the ground experiments are in fairly good agreement with the Crab observation: when their efficiencies are rescaled for a polychromatic source at infinity a peak efficiency of  $9 \pm 1\%$  is obtained. At a first glance, this figure may seem rather modest, however when considering the constraints on a compact balloon instrument, the result is actually very positive: The short focal length leads to a lens with the outermost rings occupied by crystals with high reflection orders  $n$  (see eq. 1): the outermost rings ([333] and [440] crystals) are roughly 4 times less efficient than the innermost rings ([111] and [220] crystals). Note that the largest part of the crystals is situated in the outer rings - where efficiencies are unfortunately lowest. A future space instrument will allow longer focal lengths and hence only low order crystalline planes with the highest efficiencies would be used. Also, the quality of the CLAIRE crystals was quite heterogeneous - the efficiency of the individual crystals within a ring varied by factors of 2 to 10, depending on the ring! However, the CLAIRE lens contained crystals as efficient as the Darwin model predicts: the best crystals of the lens showed peak efficiencies way above 20%.

CLAIRE's balloon flight provided the first observation of an astrophysical source with a gamma-ray lens.

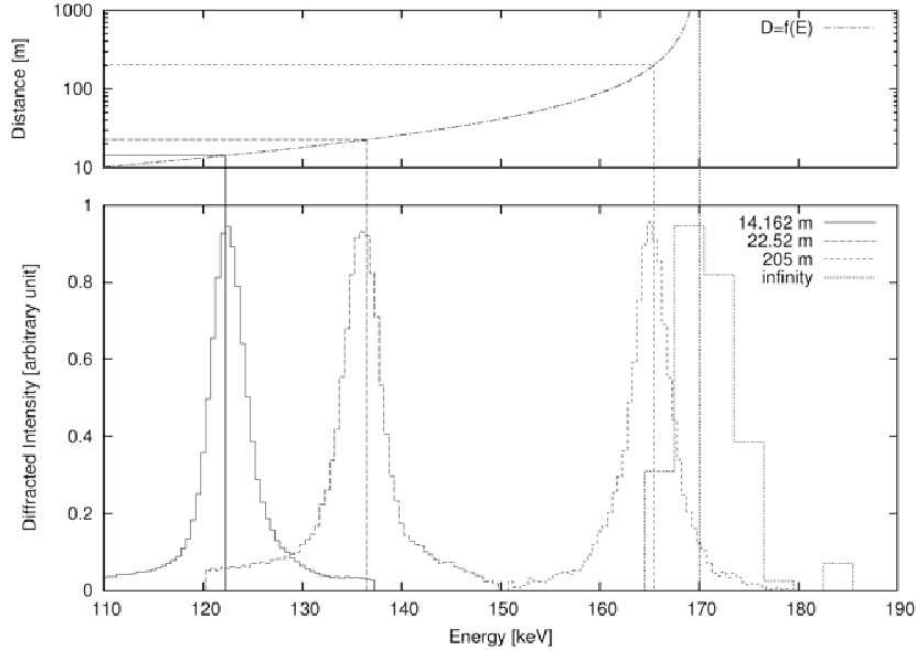


Figure 18. Recorded spectra for various source distances (lower graph). The upper graph represents the distance of the source as a function of diffracted energy. The vertical lines show the theoretical corresponding energies. 14.162 m corresponds to the tuning distance ( $E_{th}=122.29$  keV). The measurement at 22.52 m ( $E_{th}=136.5$  keV) was performed on the optical bench at CESR with a partially tuned lens. 205 m is the distance of the generator on the long distance test range ( $E_{th}=165.5$  keV). The peak for an infinite distance is taken from the stratospheric flight of June 2001.

In combination with the long-distance test on the ground, these results validate the theoretical models and demonstrate the principle of Laue lens. Moreover, CLAIRE's stratospheric flight represents a first demonstration of the Laue lens technology in space environment.

## 6.2 Current crystal development

The crystal development status is widely discussed in Refs. 24,40. Mosaic crystals of Copper are developed and produced at ILL,<sup>32</sup> mosaic crystals of  $\text{Si}_{1-x}\text{Ge}_x$  alloy with  $x$  increasing along the crystal growth axis (curved crystal) is produced at IKZ.<sup>39</sup> Crystal developments for Laue lenses are being undertaken in Italy: mosaic crystals at CNR-IMEM Institute, while curved crystals at Physics Department, University of Ferrara (see Fig. 6).

## 6.3 Current lens assembly technology development

Currently new lens assembly technologies are being developed at the University of Ferrara, for building broad bandpass (70/100-600 keV) Laue lenses, and at CESR for building high energy narrow bandpass (800-900 keV) Laue lenses.

The crystal tile positioning accuracy in the lens is the most critical issue. It depends on the mosaic spread and focal length. Higher focal lengths require higher positioning accuracies, thus the development is more challenging for lenses working at the highest energies.

### 6.3.1 Assembly technology status for broad bandpass Laue lenses

A technology for assembling crystal tiles for a low ( $\leq 10-15$  m) focal length lens is at an advanced stage of development at the University of Ferrara.<sup>36,41,42</sup> It does not request any mechanism for a fine adjustment of the crystal orientation once the crystal is positioned in the lens frame. Using this technology, a first lens prototype with 6 m focal length has already been developed and tested. It makes use of mosaic crystals of Cu(111).



Figure 19. A view of the current configuration of the apparatus for the lens assembling. The apparatus is located in the LARIX lab of the University of Ferrara.

The technique adopted is described with details in Refs. 36,41. It makes use of a counter-mask provided with holes, two for each crystal tile. Each tile is positioned on the counter-mask by means of two cylindrical pins, rigidly glued to the crystal tile, that are inserted in the counter-mask holes. The pin direction and the axis of the average lattice plane of each crystal tile have to be exactly orthogonal. The hole axis direction constrains the energy of the photons diffracted by the tile, while the relative position of the two holes in the counter-mask establishes the azimuthal orientation of the axis of the crystal lattice plane. This axis has to cross the lens axis.

Depending on the direction of the hole axes in the counter-mask, the desired geometry of lens can be obtained. In the case of a lens for space astronomy, the hole axes have to be directed toward the center of curvature of the lens. In the case of the developed prototype, the hole axes were set parallel to the lens axis for the quick test of the lens with an X-ray tube, that provide a highly divergent X-ray beam.

Once all the crystal tiles are placed on the counter-mask, a frame is glued to the entire set of the crystals. Then the lens frame, along with the crystals, is separated from the counter-mask and from the pins. In the case of first prototype, instead of using a chemical attack in order to separate the counter-mask from the lens as foreseen in the project, a mechanical separation was attempted.

The first developed prototype was made of a 36 cm diameter ring of 20 mosaic crystal tiles. The mosaic spread of the used crystals ranged from  $\sim 2.5$  and  $\sim 3.5$  arcmin. The tile cross-section was  $15 \times 15 \text{ mm}^2$  while its thickness was 2 mm. The lens frame was made of carbon fibers with a total thickness of 1 mm.

The X-ray beam used first to assemble the crystals in the lens and then to test it, is that available in the LARIX (LArge Italian hard X-ray) facility of the University of Ferrara. For a LARIX description see Ref. 43. A view of the experimental apparatus in the current configuration is shown in Fig. 19.

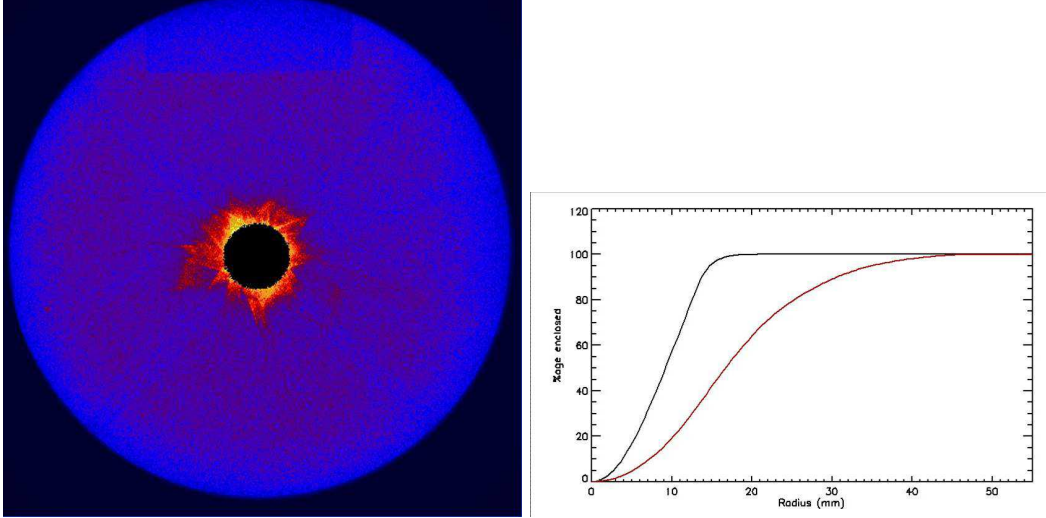


Figure 20. *Left panel:* difference between the PSF measured and that obtained with a Monte Carlo code by assuming a perfect positioning of the crystal tiles in the lens. *Right panel:* cumulative distribution of the focused photons as a function of radial distance from the focal point. *Black line:* expected distribution in the case of a perfect positioning of the crystal tiles in the lens. *Red line:* measured distribution. Reprinted from Ref. 36.

The prototype was widely tested using the polychromatic X-ray beam described above, as reported in the Ref. 36. Figure 20 shows difference between the measured PSF and that obtained from a simulation, in which a perfect positioning of the crystals in the lens was assumed. As can be seen, only the center part of the measured image (i.e., the black region) is subtracted by the simulated image. The corona still visible in the difference image is the result of the cumulative error (mainly that due to the mechanical separation of the lens from the counter mask) during the lens assembly process.

The disagreement between the measured and the expected PSF is also apparent by comparing the cumulative distribution of the photons with the distance from the lens focus (see Fig. 20, right panel). As it can be seen, the PSF radius at which the expected fraction of focused photons reach the saturation (16 mm) corresponds to  $\sim 60\%$  of the measured fraction.

The spectrum of the reflected photons by developed prototype is shown in Fig. 21, where we compare the measured spectrum of the central region (i.e., photons in the black region of the left panel of Fig. 20) with the spectrum of all reflected photons. As can also be seen from this figure, the centroid of the spectrum of the central region achieves an intensity level 0.8 times that of the peak spectrum of all reflected photons.

A new prototype is being developed that takes into account the experience gained with the first one.<sup>42</sup>

#### 6.4 R&D for a tunable narrow bandpass lens

Observing in *only one* narrow energy band might be considered too much of a handicap for a space instrument using a narrow bandpass Laue lens. In the framework of an R&D project for the French Space Agency CNES, a tunable  $\gamma$ -ray lens prototype (Fig. 22 a) was developed and demonstrated.<sup>44</sup> The capability to observe more than one astrophysical line with a narrow bandpass Laue lens requires the tuning of two parameters: the Bragg angle  $\theta_B$  and the focal distance  $f$ . While the focal  $f$  will have to be controlled to within  $\sim 1$  cm, the precision of the crystal inclination has to be better than the mosaic structure of the crystals. In the setup of Ref. 44, each crystal was tuned by using piezo-driven actuators to change the crystal inclination, and an eddy-current sensor to determine the current position (Fig. 22a). The resolution of the control-loop permitted an angular resolution of 0.1–0.4 arcsec. The stability was found to be better than 0.8 arcsec per day and the reproducibility of a particular tuning better than 5 arcsec over a 10 day period (Fig. 22b).

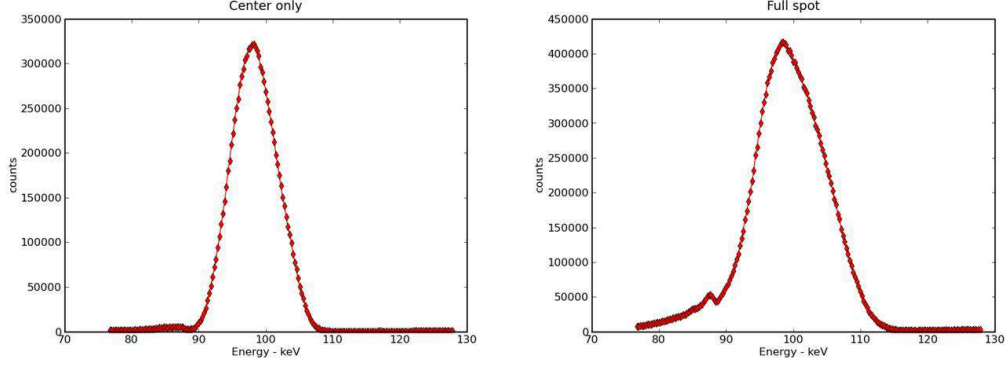


Figure 21. *Left panel:* photon spectrum of the region (see left panel of Fig. 20) in which all the reflected photons are expected to be found in the case of a perfect mounting of the crystal tiles in the lens. *Right panel:* spectrum of all reflected photons. Reprinted from Ref. 36.

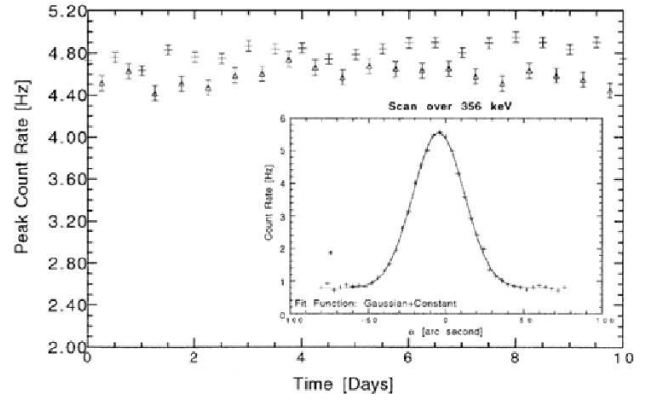
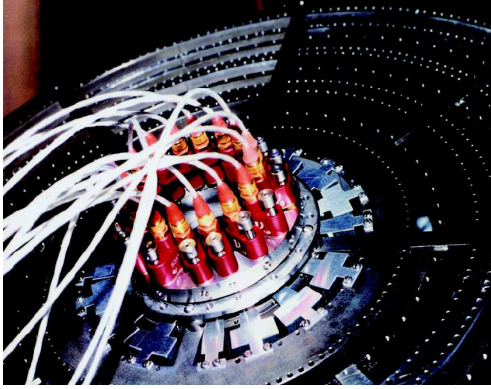


Figure 22. a) Prototype tunable lens. b) The evolution in time of the peak count rate when alternatively focusing 303 keV (circles) and 356 keV (crosses)  $\gamma$ -rays demonstrates the stability and reproducibility of the lens tuning.

## 7. PROSPECTS AND CONCLUSIONS

A big effort has already been performed and is still in progress for the development of focusing Laue lenses for gamma-ray astronomy ( $>70/100$  keV). Thanks to the most recent developments, Laue lenses with low focal length (10–15 m) are already feasible. The major task now in progress is the development of the crystals needed to optimize the lens effective area. A project "LAUE", supported by the Italian Space Agency, has just started in Italy (main contractor DTM, Modena) for the development of both suitable Laue lens crystals and an advanced assembly technology of high focal length lenses (up to 100 m).

Thus far, the major limit to the launch of a Laue lens gamma-ray telescope has been the need of high focal length (20–100 m), that implies the use of two satellites in formation flying, one for the lens, and the other for the focal plane detector. The development of extendable booms up to 20 m, the optimization of the lens effective area and the limitation of the lens bandpass to lower energies, all make realistic the prospect of broad band satellite missions that could join together multilayer mirrors and Laue lenses to extend the focusing band up to several hundreds of keV.

Just as an example, the  $10^5$  s continuum sensitivity of a Laue lens made of mosaic crystals, that was investigated by Ref. 28 and mentioned above (see sect. 4.5.2), is shown in Fig. 23. The use of curved crystals can further increase the lens sensitivity.

In the framework of formation flying missions, the mission concept DUAL (Ref. 45) is currently under study by a consortium of institutes from Europe, Japan and the USA. The DUAL mission is composed of a Wide-field Compton telescope (WCT) which carries out all-sky surveys, and a narrow band (800–900 keV)



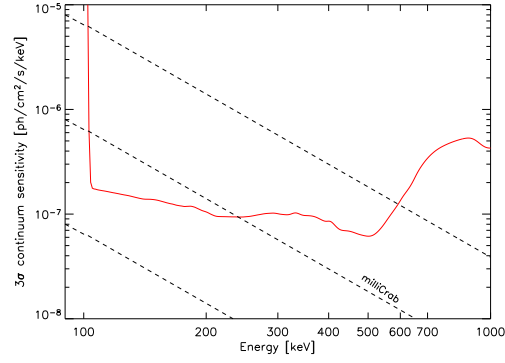


Figure 23.  $3\sigma$  continuum sensitivity ( $\Delta E = E/2$ ) of the lens discussed in Section 4.5.2 for 100 ks observation time. Reprinted from Ref. 28.

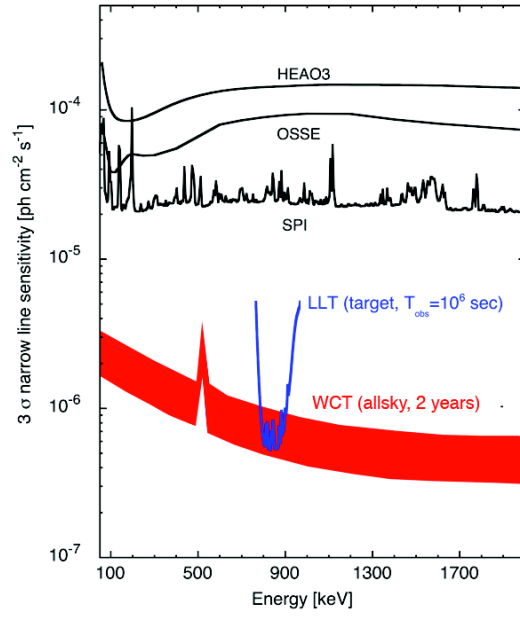


Figure 24. Sensitivity estimation of DUAL's Laue Lens Telescope (LLT, red curve), enabling study of SNe Ia out to 50-80 Mpc, for dozens of potential targets each year. Also shown is the estimated survey sensitivity (two years) of the Wide Field Compton Telescope (WCT, blue curve) which serves as a focal plane detector of the LLT.

Laue-Lens Telescope (LLT) that simultaneously performs very deep observations of selected narrow-field targets. Combining a small Compton telescope with a Laue lens will permit to solve the apparently contradictory needs for a future gamma-ray mission : map out large-scale distributions, monitor extreme accelerators, and measure the polarization of gamma-ray bursts with a small medium-sensitivity Compton Camera and simultaneously accomplish the stringent performance requirements for the specific science goal of SN1a thanks to the Laue Lens. A compact, wide field ( $2\text{--}3\pi$  steradian) Compton telescope with a modest geometric area ( $400\text{--}1600\text{ cm}^2$ ) resulting in a effective area of  $40\text{--}160\text{ cm}^2$  can fulfill the needs for the "all-sky science" and simultaneously serve as a focal plane detector for the LLT. A Laue lens that can achieve sensitivities  $10^{-6}\text{ photons cm}^{-2}\text{ s}^{-1}$  to a 3% broadened line at 847 keV can be made from Au, Ag and Cu crystals, similar to the ones presently measured. The model lens used for the sensitivity shown in Fig. 24 would have a focal length of the order of 68 m, a radius of 40-58 cm and a total mass of 40 kg.

We expect that future broad band X-/gamma-ray missions for the deep study of non thermal astrophysical processes above 100 keV, antimatter annihilation signatures, and nuclear lines from SN explosions will include Laue lenses.

## ACKNOWLEDGMENTS

FF acknowledges the financial support by the Italian Space Agency ASI. PvB acknowledges continuing support from the French Space Agency CNES, and is particularly grateful to the balloon division of CNES which built the pointing system and operated the CLAIRE flights from the launch to the gondola recovery.

## REFERENCES

- [1] Winkler, C., Gehrels, N., Schönfelder, V., Roques, J., Strong, A. W., Wunderer, C., Ubertini, P., Lebrun, F., Bazzano, A., Del Santo, M., Lund, N., Westergaard, N. J., Beckmann, V., Kretschmar, P., and Mereghetti, S., "First results from the INTEGRAL galactic plane scans," *A&A* **411**, L349–L355 (Nov. 2003).
- [2] Gehrels, N., Chincarini, G., Giommi, P., Mason, K. O., Nousek, J. A., Wells, A. A., White, N. E., Barthelmy, S. D., Burrows, D. N., Cominsky, L. R., Hurley, K. C., Marshall, F. E., Mészáros, P., Roming, P. W. A., Angelini, L., Barbier, L. M., Belloni, T., Campana, S., Caraveo, P. A., Chester, M. M., Citterio, O., Cline, T. L., Cropper, M. S., Cummings, J. R., Dean, A. J., Feigelson, E. D., Fenimore, E. E., Frail, D. A., Fruchter, A. S., Garmire, G. P., Gendreau, K., Ghisellini, G., Greiner, J., Hill, J. E., Hunsberger, S. D., Krimm, H. A., Kulkarni, S. R., Kumar, P., Lebrun, F., Lloyd-Ronning, N. M., Markwardt, C. B., Mattson, B. J., Mushotzky, R. F., Norris, J. P., Osborne, J., Paczynski, B., Palmer, D. M., Park, H., Parsons, A. M., Paul, J., Rees, M. J., Reynolds, C. S., Rhoads, J. E., Sassee, T. P., Schaefer, B. E., Short, A. T., Smale, A. P., Smith, I. A., Stella, L., Tagliaferri, G., Takahashi, T., Tashiro, M., Townsley, L. K., Tueller, J., Turner, M. J. L., Vietri, M., Voges, W., Ward, M. J., Willingale, R., Zerbi, F. M., and Zhang, W. W., "The Swift Gamma-Ray Burst Mission," *ApJ* **611**, 1005–1020 (Aug. 2004).
- [3] Bird, A. J., Bazzano, A., Bassani, L., Capitanio, F., Focchi, M., Hill, A. B., Malizia, A., McBride, V. A., Scaringi, S., Sguera, V., Stephen, J. B., Ubertini, P., Dean, A. J., Lebrun, F., Terrier, R., Renaud, M., Mattana, F., Götz, D., Rodriguez, J., Belanger, G., Walter, R., and Winkler, C., "The Fourth IBIS/ISGRI Soft Gamma-ray Survey Catalog," *ApJS* **186**, 1–9 (Jan. 2010).
- [4] Cusumano, G., La Parola, V., Segreto, A., Mangano, V., Ferrigno, C., Maselli, A., Romano, P., Mineo, T., Sbarufatti, B., Campana, S., Chincarini, G., Giommi, P., Masetti, N., Moretti, A., and Tagliaferri, G., "The Palermo Swift-BAT Hard X-ray Catalogue. II- Results after 39 months of sky survey," *ArXiv e-prints* (June 2009).
- [5] Weidenspointner, G., Skinner, G., Jean, P., Knödseder, J., von Ballmoos, P., Bignami, G., Diehl, R., Strong, A. W., Cordier, B., Schanne, S., and Winkler, C., "An asymmetric distribution of positrons in the Galactic disk revealed by  $\gamma$ -rays," *Nature* **451**, 159–162 (Jan. 2008).
- [6] Diehl, R., Halloin, H., Kretschmer, K., Lichti, G. G., Schönfelder, V., Strong, A. W., von Kienlin, A., Wang, W., Jean, P., Knödseder, J., Roques, J., Weidenspointner, G., Schanne, S., Hartmann, D. H., Winkler, C., and Wunderer, C., "Radioactive  $^{26}\text{Al}$  from massive stars in the Galaxy," *Nature* **439**, 45–47 (Jan. 2006).

- [7] Frontera, F., Costa, E., dal Fiume, D., Feroci, M., Nicastro, L., Orlandini, M., Palazzi, E., and Zavattini, G., “PDS experiment on board the BeppoSAX satellite: design and in-flight performance results,” in [*EUV, X-Ray, and Gamma-Ray Instrumentation for Astronomy VIII*, Oswald H. Siegmund; Mark A. Gummin; Eds.], Siegmund, O. H. and Gummin, M. A., eds., *Presented at the Society of Photo-Optical Instrumentation Engineers (SPIE) Conference* **3114**, 206–215 (Oct. 1997).
- [8] Ubertini, P., Lebrun, F., Di Cocco, G., Bazzano, A., Bird, A. J., Broenstad, K., Goldwurm, A., La Rosa, G., Labanti, C., Laurent, P., Mirabel, I. F., Quadrini, E. M., Ramsey, B., Reglero, V., Sabau, L., Sacco, B., Staubert, R., Vigroux, L., Weisskopf, M. C., and Zdziarski, A. A., “IBIS: The Imager on-board INTEGRAL,” *Astron. & Astrophys.* **411**, L131–L139 (2003).
- [9] Knödseder, J., von Ballmoos, P., Frontera, F., Bazzano, A., Christensen, F., Hernanz, M., and Wunderer, C., “GRI: focusing on the evolving violent universe,” in [*Optics for EUV, X-Ray, and Gamma-Ray Astronomy III*. Edited by O’Dell, Stephen L.; Pareschi, Giovanni.], *Presented at the Society of Photo-Optical Instrumentation Engineers (SPIE) Conference* **6688**, 5 (Sept. 2007).
- [10] Frontera, F., Pisa, A., de Chiara, P., and et al., “Exploring the hard X-/soft gamma-ray continuum spectra with Laue lenses,” in [*ESA Special Publication*], Favata, F., Sanz-Forcada, J., Giménez, A., and Battrick, B., eds., *ESA Special Publication* **588**, 323+ (Dec. 2005).
- [11] Frontera, F., Pisa, A., Carassiti, V., Evangelisti, F., Loffredo, G., Pellicciotta, D., Andersen, K. H., Courtois, P., Amati, L., Caroli, E., Franceschini, T., Landini, G., Silvestri, S., and Stephen, J. B., “Gamma-ray lens development status for a European gamma-ray imager,” in [*Space Telescopes and Instrumentation II: Ultraviolet to Gamma Ray*], Turner, M. J. L. and Hasinger, G., eds., *Presented at the Society of Photo-Optical Instrumentation Engineers (SPIE) Conference* **6266** (July 2006).
- [12] Knödseder, J., “GRI: the gamma-ray imager mission,” in [*Space Telescopes and Instrumentation II: Ultraviolet to Gamma Ray*. Edited by Turner, Martin J. L.; Hasinger, Günther. *Proceedings of the SPIE, Volume 6266*, pp. 626623 (2006).], Turner, M. J. L. and Hasinger, G., eds., *Presented at the Society of Photo-Optical Instrumentation Engineers (SPIE) Conference* **6266** (July 2006).
- [13] Götz, D., Mereghetti, S., Tiengo, A., and Esposito, P., “Magnetars as persistent hard X-ray sources: INTEGRAL discovery of a hard tail in SGR 1900+14,” *A&A* **449**, L31–L34 (Apr. 2006).
- [14] Kuiper, L., Hermsen, W., den Hartog, P. R., and Collmar, W., “Discovery of Luminous Pulsed Hard X-Ray Emission from Anomalous X-Ray Pulsars 1RXS J1708-4009, 4U 0142+61, and 1E 2259+586 by INTEGRAL and RXTE,” *ApJ* **645**, 556–575 (July 2006).
- [15] Perola, G. C., Matt, G., Cappi, M., Fiore, F., Guainazzi, M., Maraschi, L., Petrucci, P. O., and Piro, L., “Compton reflection and iron fluorescence in BeppoSAX observations of Seyfert type 1 galaxies,” *A&A* **389**, 802–811 (July 2002).
- [16] Risaliti, G., “The BeppoSAX view of bright Compton-thin Seyfert 2 galaxies,” *A&A* **386**, 379–398 (May 2002).
- [17] Ghisellini, G., Della Ceca, R., Volonteri, M., Ghirlanda, G., Tavecchio, F., Foschini, L., Tagliaferri, G., Haardt, F., Pareschi, G., and Grindlay, J., “Chasing the heaviest black holes of jetted Active Galactic Nuclei,” *ArXiv e-prints* (Nov. 2009).
- [18] Rephaeli, Y., Nevalainen, J., Ohashi, T., and Bykov, A. M., “Nonthermal Phenomena in Clusters of Galaxies,” *Space Science Reviews* **134**, 71–92 (Feb. 2008).
- [19] Gilli, R., Comastri, A., and Hasinger, G., “The synthesis of the cosmic X-ray background in the Chandra and XMM-Newton era,” *A&A* **463**, 79–96 (Feb. 2007).
- [20] Goldwurm, A., Ballet, J., Cordier, B., Paul, J., Bouchet, L., Roques, J. P., Barret, D., Mandrou, P., Sunyaev, R., Churazov, E., Gilfanov, M., Dyachkov, A., Khavenson, N., Kovtunenkov, V., Kremnev, R., and Sukhanov, K., “Sigma/GRANAT soft gamma-ray observations of the X-ray nova in Musca - Discovery of positron annihilation emission line,” *ApJ* **389**, L79–L82 (Apr. 1992).
- [21] Zachariasen, W. H., [*Theory of X-rays Diffraction in Crystals*], J. Wiley, New York (1945).
- [22] Pellicciotta, D., Frontera, F., Loffredo, G., Pisa, A., Andersen, K., Courtois, P., Hamelin, B., Carassiti, V., Melchiorri, M., and Squerzanti, S., “Laue Lens Development for Hard X-rays (>60 keV),” *IEEE Trans. Nucl. Sci.* **53**, 253–258 (2006).
- [23] Authier, A., [*Dynamical Theory of X-ray Diffraction*], Oxford University Press, Oxford (2001).



- [24] Barriere, N., Rousselle, J., von Ballmoos, P., Abrosimov, N. V., Courtois, P., Bastie, P., Camus, T., Jentschel, M., Kurlov, V. N., Natalucci, L., Roudil, G., Frisch Brejnholt, N., and Serre, D., "Experimental and theoretical study of diffraction properties of various crystals for the realization of a soft gamma-ray Laue lens," *Journal of Applied Crystallography* **42**, 834–845.
- [25] Keitel, S., Malgrange, C., Niemoeller, T., and Schneider, J. R., "Diffraction of 100 to 200 keV from an  $\text{Si}_{1-x}\text{Ge}_x$  gradient crystal: comparison with results from dynamical theory," *Acta Crystallographica A* **55**, 855–863 (1999).
- [26] Malgrange, V., "X-ray Propagation in Distorted Crystals: From Dynamical to Kinematical Theory," *Crystals research and technology* **37**, 654–662 (2002).
- [27] Barriere, N., *Developpement d'une lentille de Laue pour l'astrophysique nucleaire*, PhD thesis, University of Toulouse, France (2008).
- [28] Barrière, N. M., Natalucci, L., Abrosimov, N., von Ballmoos, P., Bastie, P., Courtois, P., Jentschel, M., Knödlseider, J., Rousselle, J., and Ubertini, P., "Soft gamma-ray optics: new Laue lens design and performance estimates," in [*Society of Photo-Optical Instrumentation Engineers (SPIE) Conference Series*], *Presented at the Society of Photo-Optical Instrumentation Engineers (SPIE) Conference* **7437** (Aug. 2009).
- [29] Pisa, A., Frontera, F., De Chiara, P., Loffredo, G., Pellicciotta, D., Landini, G., Franceschini, T., Silvestri, S., Andersen, K., Courtois, P., and Hamelin, B., "Feasibility study of a Laue lens for hard x rays for space astronomy," in [*Advances in Computational Methods for X-Ray and Neutron Optics. Edited by Sanchez del Rio, Manuel.*], Sanchez del Rio, M., ed., *Presented at the Society of Photo-Optical Instrumentation Engineers (SPIE) Conference* **5536**, 39–48 (Oct. 2004).
- [30] Pisa, A., Frontera, F., De Chiara, P., Loffredo, G., Pellicciotta, D., Carassiti, V., Evangelisti, F., Andersen, K., Courtois, P., Hamelin, B., Amati, L., Landini, G., Franceschini, T., and Silvestri, S., "Development status of a Laue lens for high energy x-rays (>60 keV)," in [*Optics for EUV, X-Ray, and Gamma-Ray Astronomy II*], Citterio, O. and O'Dell, S. L., eds., *Presented at the Society of Photo-Optical Instrumentation Engineers (SPIE) Conference* **5900**, 350–359 (Aug. 2005).
- [31] Pisa, A., Frontera, F., Loffredo, G., Pellicciotta, D., and Auricchio, N., "Optical properties of Laue lenses for hard X-rays (>60 keV)," *Experimental Astronomy* **20**, 219–228 (Dec. 2005).
- [32] Courtois, P., Andersen, K. H., and Bastie, P., "Copper Mosaic Crystals for Laue Lenses," *Experimental Astronomy* **20**, 195–200 (Dec. 2005).
- [33] Lund, N., "A study of focusing telescopes for soft gamma rays," *Experimental Astronomy* **2**, 259–273 (1992).
- [34] Lindquist, T. R. and Webber, W. R., "A focusing X-ray telescope for use in the study of extraterrestrial X-ray sources in the energy range 20-140 keV," *Canadian Journal of Physics* **46**, 1103–+ (1968).
- [35] Frontera, F., Loffredo, G., Pisa, A., Virgili, E., Carassiti, V., Evangelisti, F., Landi, L., Squerzanti, S., Auricchio, N., Caroli, E., Landini, G., Silvestri, S., and Stephen, J. B., "A gamma-ray Laue lens focusing telescope aboard a balloon experiment," *Memorie della Societa Astronomica Italiana* **79**, 807–811 (2008).
- [36] Frontera, F., Loffredo, G., Pisa, A., Nobili, F., Carassiti, V., Evangelisti, F., Landi, L., Squerzanti, S., Caroli, E., Stephen, J. B., Andersen, K. H., Courtois, P., Auricchio, N., Milani, L., and Negri, B., "Focusing of gamma-rays with Laue lenses: first results," in [*Society of Photo-Optical Instrumentation Engineers (SPIE) Conference Series*], *Society of Photo-Optical Instrumentation Engineers (SPIE) Conference Series* **7011** (Aug. 2008).
- [37] von Ballmoos, P., Halloin, H., Evrard, J., Skinner, G., Abrosimov, N., Alvarez, J., Bastie, P., Hamelin, B., Hernanz, M., Jean, P., Knödlseider, J., and Smither, B., "CLAIRE: First light for a gamma-ray lens," *Experimental Astronomy* **20**, 253–267 (Dec. 2005).
- [38] Alvarez, J., Halloin, H., Hernanz, M., von Ballmoos, Jean, P., Skinner, G., and Abrosimov, N., "Long Distance Test of the CLAIRE Gamma-Ray Lens," in [*Proc 5th INTEGRAL Workshop (ESA SP-552)*], (2004).
- [39] Abrosimov, N. V., "Mosaic and gradient SiGe single crystals for gamma ray Laue lenses," *Experimental Astronomy* **20**, 185–194 (Dec. 2005).
- [40] Rousselle, J., von Ballmoos, P., Barrière, N., Abrosimov, N. V., Bastie, P., Bonnetto, G., Camus, T., Courtois, P., Jentschel, M., Lecomte, E., Rivière, E., and Roudil, G., "High-Z crystals for gamma-ray optics," in [*Society of Photo-Optical Instrumentation Engineers (SPIE) Conference Series*], *Presented at the Society of Photo-Optical Instrumentation Engineers (SPIE) Conference* **7437** (Aug. 2009).

- [41] Frontera, F., Loffredo, G., Pisa, A., Milani, L., Nobili, F., Auricchio, N., Carassiti, V., Evangelisti, F., Landi, L., Squerzanti, S., Andersen, K. H., Courtois, P., Amati, L., Caroli, E., Landini, G., Silvestri, S., Stephen, J. B., Poulsen, J. M., Negri, B., and Pareschi, G., “Development status of a Laue lens project for gamma-ray astronomy,” in [*Optics for EUV, X-Ray, and Gamma-Ray Astronomy III. Edited by O’Dell, Stephen L.; Pareschi, Giovanni. Proceedings of the SPIE*], Presented at the Society of Photo-Optical Instrumentation Engineers (SPIE) Conference **6688**, 20 (2007).
- [42] Ferrari, F., Frontera, F., Loffredo, G., Virgilli, E., Guidorzi, C., Carassiti, V., Evangelisti, F., Landi, L., Chiozzi, S., Squerzanti, S., Caroli, E., Stephen, J. B., Schiavone, F., Basili, A., Andersen, K. H., and Courtois, P., “New results on focusing of gamma-rays with Laue lenses,” in [*Society of Photo-Optical Instrumentation Engineers (SPIE) Conference Series*], Presented at the Society of Photo-Optical Instrumentation Engineers (SPIE) Conference **7437** (Aug. 2009).
- [43] Loffredo, G., Frontera, F., Pellicciotta, D., Pisa, A., Carassiti, V., Chiozzi, S., Evangelisti, F., Landi, L., Melchiorri, M., and Squerzanti, S., “The Ferrara hard X-ray facility for testing/calibrating hard X-ray focusing telescopes,” *Experimental Astronomy* **20**, 413–420 (Dec. 2005).
- [44] Kohnle, A., Smither, R., Graber, T., von Ballmoos, P., Laporte, P., and Olive, J. F., “Realization of a tunable crystal lens as an instrument to focus gamma rays,” *Nuclear Instruments and Methods in Physics Research A* **408**, 553–561 (May 1998).
- [45] von Ballmoos, P., Takahashi, T., and Boggs, S., “A DUAL mission for nuclear astrophysics,” *Nuclear Instruments and Methods in Physics Research, A*, 2010, in press, <http://dx.doi.org/10.1016/j.nima.2010.03.026> (2010).